Check for updates

A Sequential Pressure-Based Algorithm for Data-Driven Leakage Identification and Model-Based Localization in Water Distribution Networks

Ivo Daniel[1]; Jorge Pesantez, A.M.ASCE[2]; Simon Letzgus[3]; Mohammad Ali Khaksar Fasaee, S.M.ASCE[4]; Faisal Alghamdi, S.M.ASCE[5]; Emily Berglund, M.ASCE[6]; G. Mahinthakumar, M.ASCE[7]; and Andrea Cominola, A.M.ASCE[8]

Abstract: Leakages in water distribution networks (WDNs) are estimated to globally cost 39 billion USD/year and cause water and revenue losses, infrastructure degradation, and other cascading effects. Their impacts can be prevented and mitigated with prompt identification and accurate leak localization. In this work, we propose the leakage identification and localization algorithm (LILA), a pressure-based algorithm for data-driven leakage identification and model-based localization in WDNs. First, LILA identifies potential leakages via semisupervised linear regression of pairwise sensor pressure data and provides the location of their nearest sensors. Second, LILA locates leaky pipes relying on an initial set of candidate pipes and a simulation-based optimization framework with iterative linear and mixed-integer linear programming. LILA is tested on data from the L-Town network devised for the Battle of Leakage Detection and Isolation Methods. Results show that LILA can identify all leakages included in the data set and locate them within a maximum distance of 374 m from their real location. Abrupt leakages are identified immediately or within 2 h, while more time is required to raise alarms on incipient leakages. **DOI: 10.1061/(ASCE)WR.1943-5452.0001535.** © *2022 American Society of Civil Engineers.*

Author keywords: BattLeDIM; Leakage detection; Water distribution networks (WDN); Change point detection; Successive linear approximation.

Downloaded from ascelibrary.org by Andrea Cominola on 03/30/22. Copyright ASCE. For personal use only; all rights reserved.

Introduction

Water losses represent one of the major consequences of infrastructure failures in water distribution networks (WDNs) (Arregui et al. 2018). Updated estimations of water losses estimate that the global volume of nonrevenue water (NRW), or the difference between the water supplied in WDNs and the volume billed to customers, exceeds 120 billion m^3/year, with an associated economic cost of about USD 39 billion/year (Liemberger and Marin 2006). In a well-maintained WDN, background leakages and pipe bursts cause small losses on the order of 3%–7% of the total water supplied (Beuken et al. 2008). On the other hand, up to 35% of the potable water supply is lost as NRW in poorly maintained WDNs, even in developed countries (Levinas et al. 2021), and more than 50% is lost in systems in developing countries (Puust et al. 2010). Beyond water and revenue loss, pressure drops due to pipe bursts and the development of background leakages that remain hidden for a long time lead to contaminant intrusion and damage to property (Mansour-Rezaei et al. 2013). Managing NRW can yield multiple benefits, including increased operational revenues, decreased energy needs, overall improved water services, increased customer satisfaction, and reduced environmental impact, in addition to direct mitigation of the environmental and financial impact of water losses on water resources and utility operators (Wyatt et al. 2016).

Among the different strategies that utilities can adopt for NRW management, the detection of physical leaks represents a priority that has been studied in the literature for over 50 years (Puust et al. 2010). Detecting a leak in a WDN is a nontrivial problem because pressurized pipes are underground, and WDNs can branch out to form large network systems; thus, they are not easy to access for monitoring and diagnostics. Moreover, variations in water demand, seasonal trends, and measurement noise make leak detection more challenging (Sophocleous et al. 2019). Following a few early studies that focused primarily on identifying the potential factors causing leakages in WDNs (e.g., Morris 1967), the state-of-the-art literature is now rich with methods that deal with different facets of leak management. Studies have been classified by Puust et al. (2010) as methods for (1) *leakage assessment*, i.e., the estimation

[1]Graduate Student, Chair of Smart Water Networks, Technische Universität Berlin, Berlin 10623, Germany; Einstein Center Digital Future, Berlin 10117, Germany. Email: ivo.daniel@tu-berlin.de

[2]Graduate Student, Dept. of Civil, Construction, and Environmental Engineering, North Carolina State Univ., Raleigh, NC 27695. ORCID: https://orcid.org/0000-0002-1537-6006. Email: jpesant@ncsu.edu

[3]Graduate Student, Machine Learning Group, Technische Universität Berlin, Berlin 10623, Germany.

[4]Graduate Student, Dept. of Civil, Construction, and Environmental Engineering, North Carolina State Univ., Raleigh, NC 27695.

[5]Graduate Student, Dept. of Civil, Construction, and Environmental Engineering, North Carolina State Univ., Raleigh, NC 27695; Graduate Assistant, Dept. of Civil and Environmental Engineering, King Abdulaziz Univ., Jeddah, Saudi Arabia. ORCID: https://orcid.org/0000-0001-5956-7173

[6]Professor, Dept. of Civil, Construction, and Environmental Engineering, North Carolina State Univ., Raleigh, NC 27695.

[7]Professor, Dept. of Civil, Construction, and Environmental Engineering, North Carolina State Univ., Raleigh, NC 27695.

[8]Assistant Professor, Chair of Smart Water Networks, Technische Universität Berlin, Berlin 10623, Germany; Einstein Center Digital Future, Berlin 10117, Germany (corresponding author). ORCID: https://orcid.org/0000-0002-4031-4704. Email: andrea.cominola@tu-berlin.de

Note. This manuscript was submitted on April 25, 2021; approved on December 10, 2021; published online on March 30, 2022. Discussion period open until August 30, 2022; separate discussions must be submitted for individual papers. This paper is part of the ***Journal of Water Resources Planning and Management***, © ASCE, ISSN 0733-9496.

of water losses usually performed via a water balance (AWWA 2008), (2) *leakage detection*, i.e., the identification and localization of water leaks in a WDN (e.g., Levinas et al. 2021; Covas and Ramos 2010; Perez et al. 2009), and (3) *leakage control*, i.e., passive or active policies and actions to control leakages (e.g., Misiunas et al. 2005, 2006).

The ongoing digital transformation of the water industry, along with the development of distributed sensor networks and improved real-time communication, is fostering the development of a new generation of sensor-based and online, data-driven leakage detection methods that process data stored in a supervisory control and data acquisition (SCADA) system (Sarni et al. 2019; Makropoulos and Savic 2019). Acoustic devices (Stephens et al. 2018), infrared photography (Atef et al. 2016), induced pressure waves (Zeng et al. 2021), and in-pipe robots (Kazeminasab et al. 2021), for instance, have recently been tested to pinpoint the presence of leaks in a pipe or a previously defined network area. Utilities can apply on-site equipment-based methods to identify the exact position of a leak at higher resolution than computer-based models and fix it. Computer-based models, however, are not as invasive as equipment-based methods and can effectively narrow down the search area before the utility sends out a crew to localize and fix leaks. The two tasks that computer-based models need to achieve are, first, to identify the presence of a leak in the system and, second, to report the approximate location of the leak. Leak identification relies on the analysis of physical measurements, including pipe pressure and flow rates, water level in tanks, and water demand, to identify the time step when the leak occurred. Methods for leakage identification or localization usually combine hydraulic modeling with optimization techniques, e.g., genetic algorithms and search space reduction (Sophocleous et al. 2019; Vftkovsky et al. 2000; Steffelbauer et al. 2022), or data-driven algorithms based on high temporal resolution pressure or flow data (i.e., subhourly), e.g., k-nearest neighbors algorithms (Levinas et al. 2021), convolution neural networks (Fang et al. 2019; Guo et al. 2021; Bohorquez et al. 2020), Bayesian classifiers (Soldevila et al. 2017), and long short-term memory (LSTM) neural networks (Wang et al. 2020).

While several leak identification and localization methods have been demonstrated on various data sets in the literature, few applications have reached a level of maturity needed for practical implementation by water utilities (Sophocleous et al. 2019). Those methods that rely on high temporal resolution sensor data require reliable equipment for network monitoring and data communication. In addition, model-based methods also require a well-calibrated hydraulic model of the WDN and computational power to run simulations. Furthermore, most studies do not comparatively analyze and benchmark different methods and were conducted using private commercial data sets. These research and practice gaps have motivated the recent creation of a benchmark data set for leakage diagnosis in WDNs (Vrachimis et al. 2018) and the organization of the Battle of the Leakage Detection and Isolation Methods (BattLeDIM) (Vrachimis et al. 2020a). The BattLeDIM is an international competition organized for comparing the performance of leakage detection and localization methods on a common data set, with criteria based on time to detection (TTD) and location accuracy.

In this paper we present a pressure-based leakage identification and localization algorithm (LILA), formulated in its initial version for application to the BattLeDIM competition (Daniel et al. 2020). LILA is a hybrid algorithm that integrates a data-driven method for analyzing pressure data gathered with sensors distributed in a WDN and a leak localization method that relies on a calibrated hydraulic model of the WDN. The two modules operate sequentially. The first module performs leakage identification in a model-free fashion, i.e., without relying on a calibrated WDN hydraulic model. Leakage identification relies on pairwise comparison of pressure data observed at sensor nodes in the WDN and retrieved online from the SCADA system. The second module in LILA performs model-based leakage localization using a calibrated hydraulic model of the WDN and an optimization-simulation framework based on successive linear approximation (SLA) (Berglund et al. 2017).

The rest of the paper is organized as follows. In the "Methods" section, we introduce LILA and its modules for leakage identification and leakage localization. The L-Town WDN used as a case study to test LILA is presented in the section "Experimental Settings" along with the metrics for performance assessment and other experimental settings. In the "Results" section, we report and discuss the numerical results. Finally, we summarize the main conclusions and final remarks for further research in the last section.

Methods

LILA is composed of two sequential steps (Fig. 1). In the leakage identification step, a time series of raw pressure sensor data is processed to identify potential leakages in a WDN without requiring a hydraulic model of the network. When a potential leak is identified, the start time is detected and the sensor closest to the occurring leak, hereafter called the *most affected sensor* (MAS), is pinpointed.

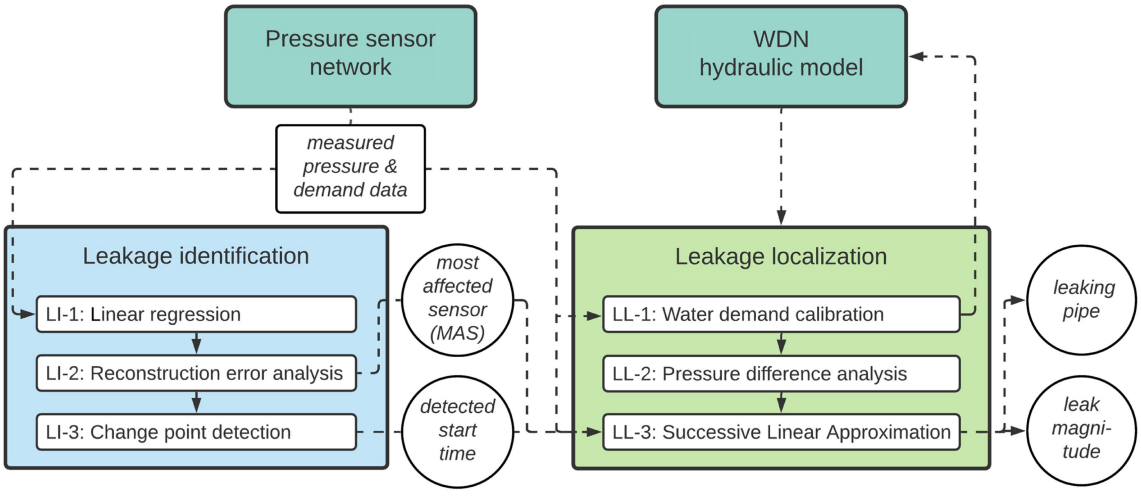

Fig. 1. Flowchart of LILA, two-step method for leakage identification and localization.

Downloaded from ascelibrary.org by Andrea Cominola on 03/30/22. Copyright ASCE. For personal use only; all rights reserved.

Second, knowledge about the MAS and the leak start time is employed for leakage localization, utilizing a hydraulic model of the WDN. In this step, the specific pipe where the leakage occurs is identified and the magnitude of the leak is determined.

The leakage identification step is designed to raise an alarm about the presence of a potential leak. After calibration of a linear regression model on pressure data from different sensors distributed in the WDN, the model can analyze new data in an online fashion without any restriction on the time resolution of the data. The observed pressure data are then compared to the model output, and the model reconstruction error (MRE) is further analyzed for the detection of change points. An alarm is raised when a change point is detected. Moreover, the identification model provides localization information at a coarse level by estimating the MAS. The leakage localization step relies on a well-calibrated hydraulic simulation model of the WDN to determine the most approximate leakage location and magnitude. An optimization-simulation model is implemented to minimize the absolute difference between observed and simulated pressure, where the solution corresponds to the pipe that caused a discrepancy between observed and simulated pressure values (Berglund et al. 2017).

Note that the information transferred from the leakage identification to the leakage localization step, i.e., the start time of the identified leak and the corresponding MAS, provides a starting condition to facilitate the search of the leakage localization process. In principle, each step could be performed detached from the other. However, the synergies of timely identification and precise localization of leakages emerge from their combination, as implemented in LILA. The two steps of leakage identification and leakage localization are described in detail as follows.

Leakage Identification

LI-1: Linear Regression

The leakage identification step originates from the principle of energy conservation at node pairs i and j based on the Bernoulli equation (Walski et al. 2003)

$$Z_i + \frac{P_i}{\gamma} + \frac{v_i^2}{2g} + \sum h_{\text{loss},i} = Z_j + \frac{P_j}{\gamma} + \frac{v_j^2}{2g} + \sum h_{\text{loss},j} \quad (1)$$

where Z = geodetic height; P = pressure; v = velocity; h_{loss} = head losses; γ = fluid specific weight; and g = gravitational constant. The meaning of each variable in Eq. (1) and the following ones is also reported in the notation section. The head losses h_{loss} account for both pipe friction losses h_{friction} and minor losses h_{minor}. These can be estimated according to Walski et al. (2003) as

$$\sum h_{\text{loss},i} = \sum h_{\text{friction},i} + \sum h_{\text{minor},i} = \sum_{p \in F_i} (k_p^{fr} + k_p^m) Q_p^2 \quad (2)$$

where $p \in F_i$ = all pipes p included in flow path F_i to node i; k_p^{fr} = frictional loss coefficient; k_p^m = minor loss coefficient; and Q_p = volumetric flow rate in pipe p.

When considering regular demand patterns throughout the network, as in Cominola et al. (2018), i.e., $Q_i \sim Q_p$, $\forall p \in F_i$, and, thus, $v_i \sim v_p$, the flow in each pipe $p \in F_i$ and the pressure P_i in the current node i have a quadratic dependency [see relation in Eq. (1) considering sensors i and pipe p], such that

$$P_i \sim -Q_p^2, \quad \forall\ p \in F_i \quad (3)$$

While Eq. (3) holds true, it can be applied to Eq. (2) in the form of linear regression, yielding

$$\sum h_{\text{loss},i} = \sum_{p \in F_i} (k_p^{fr} + k_p^m) Q_p^2 = \sum_{p \in F_i} (k_p^0 + k_p^1 P_i) = \overline{k_{p,i}^0} + \overline{k_{p,i}^1} P_i \quad (4)$$

where k_p^0 and k_p^1 = regression coefficients relating to losses in each pipe; and $\overline{k_{p,i}^0}$ and $\overline{k_{p,i}^1}$ = summarized coefficients.

Irregular (e.g., nonrecurrent) demand patterns can be regarded separately if their flow pattern is known. In this case, Eq. (4) extends to

$$\sum h_{\text{loss},i} = \overline{k_{p,i}^0} + \overline{k_{p,i}^1} P_i + \sum_{d \in D_{IR}} k_{d,i} Q_d^2 \quad (5)$$

where $d \in D_{IR}$ = all demands d from the set of irregular demands D_{IR}; and $k_{d,i}$ = partial loss coefficient for flow in pipe p in path to node i from Eq. (2) with regard to particular flow Q_d caused by demand d. Moreover, the kinetic energy term from Eq. (1) can be estimated according to Eq. (3), introducing additional regression constants $k_{E,i}^0$ and $k_{E,i}^1$

$$\frac{v_i^2}{2g} = \frac{Q_i^2}{2g \cdot \mathcal{A}_i^2} = k_{E,i}^0 + k_{E,i}^1 P_i \quad (6)$$

Combining Eqs. (1), (5), and (6) yields

$$Z_i + \frac{P_i}{\gamma} + k_{E,i}^0 + k_{E,i}^1 P_i + \overline{k_{p,i}^0} + \overline{k_{p,i}^1} P_i + \sum_{d \in D_{IR}} k_{d,i} Q_d^2 = Z_j + \frac{P_j}{\gamma} + k_{E,j}^0 + k_{E,j}^1 P_j + \overline{k_{p,j}^0} + \overline{k_{p,j}^1} P_j + \sum_{d \in D_{IR}} k_{d,j} Q_d^2 \quad (7)$$

and rearranging into

$$P_i = \frac{\Delta Z_{ji} + \Delta k_{E,ji}^0 + \Delta \overline{k_{p,ji}^0}}{\frac{1}{\gamma} + k_{E,i}^0 + \overline{k_{p,i}^1}} + P_j \frac{\frac{1}{\gamma} + k_{E,j}^0 + \overline{k_{p,j}^1}}{\frac{1}{\gamma} + k_{E,i}^0 + \overline{k_{p,i}^1}} + \frac{\sum_{d \in D_{IR}} \Delta k_{d,ji} Q_d^2}{\frac{1}{\gamma} + k_{E,i}^0 + \overline{k_{p,i}^1}} \quad (8)$$

enables the formulation of the linear regression model of the pressure signals from two sensor nodes P_i and P_j, including irregular demand D_{IR} as additional regression variables. The regression coefficients k_{ji}^0, k_{ji}^1, and k_{ji}^d can be estimated as

$$k_{ji}^0 = \frac{\Delta Z_{ji} + \Delta k_{E,ji}^0 + \Delta \overline{k_{p,ji}^0}}{\frac{1}{\gamma} + k_{E,i}^0 + \overline{k_{p,i}^1}} \quad (9)$$

$$k_{ji}^1 = \frac{\frac{1}{\gamma} + k_{E,j}^0 + \overline{k_{p,j}^1}}{\frac{1}{\gamma} + k_{E,i}^0 + \overline{k_{p,i}^1}} \quad (10)$$

and

$$k_{ji}^d = \frac{\Delta k_{d,ji}}{\frac{1}{\gamma} + k_{E,i}^0 + \overline{k_{p,i}^1}}, \quad \forall\ d \in D_{IR} \quad (11)$$

Hence, we can reformulate Eq. (8) in a simplified fashion fitting to the linear regression problem

$$P_i = k_{ji}^0 + P_j k_{ji}^1 + \sum_{d \in D_{IR}} k_{ji}^d Q_d^2 \quad (12)$$

Downloaded from ascelibrary.org by Andrea Cominola on 03/30/22. Copyright ASCE. For personal use only; all rights reserved.

During model calibration, regression coefficients k^0_{ji}, k^1_{ji}, and k^d_{ji} are estimated using a least-squares method (Montgomery 2020) on a manually selected time period where no leaks have occurred.

LI-2: Reconstruction Error Analysis

When comparing the time series of the node pressure estimated with the linear regression model $\hat{P}_i$ formulated in Eq. (12) with the observed pressure values P_i by analyzing their difference [compare Eq. (13)], additional occurring flows, i.e., leakages, contribute to an increase of the model error. They can be regarded in Eq. (12) as part of additional demand in the WDN. This yields the following definition of the MRE:

$$\mathrm{MRE}_{ji} = P_i - \hat{P}_i = P_i - \left(k^0_{ji} + P_j k^1_{ji} + \sum_{d\in D_{IR}} k_{d,ji} Q^2_d\right) = \sum_{l\in L} k_{l,ji} Q^2_l \tag{13}$$

where L denotes all leakages. Under the assumptions that no leakages are present in the network and that measurement noise is white noise, MRE is expected to be normally distributed with a mean value of 0 for all time steps $t_{\text{no leak}}$. Its expectation value $E(\cdot)$ will be $E[\mathrm{MRE}_{ji}(t_{\text{no leak}})] = 0$.

The pressure drop $\Delta P = P(t_{\text{leak}}) - P(t_{\text{no leak}})$ caused at a certain location in the WDN by a leakage can be calculated as the difference of the pressure value observed at that location in the two time steps before ($t_{\text{no leak}}$) and after (t_{leak}) the leak start. Considering a leakage l_s occurring at a location with corresponding MAS s, the pressure drop at s due to the leakage will be greater in magnitude than for all other sensor locations. Because the pressure drop is negative in sign, the following relation is obtained:

$$\Delta P_s < \Delta P_i, \quad \forall\ i \neq s \tag{14}$$

When combining Eqs. (13) and (14) and choosing $s = j$, the effect of the leakage l_s will cause exclusively positive trends in the MRE_{si}, such that $E[\mathrm{MRE}_{si}(t_{\text{leak}})] > 0$, $\forall i \neq s$, thereby enabling identification of the MAS

$$s(t) = \arg\max_j \left(\sum_i \mathrm{sign}(\mathrm{MRE}_{ji}(t))\right) \tag{15}$$

Furthermore, let the vector MRE_s be represented by the MRE for the combination of node s with all nodes i; then the magnitude of that vector may be calculated with the Frobenius-norm $\|\cdot\|_F$ (cf. Golub and Van Loan 2013). Finally, the detection of a single new leak occurring in the WDN, along with its starting time, may be accomplished by applying change point detection (Step LI-3) to the time series $\|\mathrm{MRE}_s(t)\|_F$. After a leak is definitively identified and becomes distinct, the model may be recalibrated to be reset for new leakage identification.

Multiple simultaneous leaks will also be reflected in the time series $\|\mathrm{MRE}_s(t)\|_F$ in an aggregated form [compare Eq. (13)]. However, disaggregation into individual leaks is not straightforward in the current implementation of LILA. Thus, for a more precise analysis of each individual leak within the overall aggregated error, we manually selected, for each leak, an individual combination of nodes that revealed the leak signal in the most distinct fashion.

LI-3: Change Point Detection

The last task of leakage identification is the detection of variations in the MRE time series induced by a leak flow; therefore, this represents a change point detection problem. Change point detection problems have been widely studied in the literature, and there is a multitude of statistical methods available. For a comprehensive review we refer the reader to Aminikhanghahi and Cook (2017). As explained in the previous section, we expect the MRE to be unbiased and normally distributed for the network state without leaks. With the start of a leak event, the error mean will either abruptly or gradually shift away from zero, depending on the nature of the leak. Successful change point detection aims to flag these instances as early as possible, while at the same time avoiding false alarms. In LILA, we apply the widely used Cusum algorithm (Montgomery 2020), known from statistical process monitoring, to automatically detect changes in the MRE.

The Cusum algorithm is a method to detect changes in the probability distribution of an univariate signal. It accumulates the distance C_i of the target variable x from its mean μ_x, corrected by a slack value K, which is chosen based on the change of mean that is to be detected. Often K is selected based on the estimated standard deviation σ^*_x of the target variable multiplied by a parameter δ [cf. Eq. (16)]. A change point is flagged once C_i exceeds a predefined threshold $H = \eta \times \sigma_x$. In general, the algorithm comes in two forms for detecting positive and negative changes from the mean. For our application, we use the formulation to detect changes in the positive direction because leaks will manifest themselves as positive values in the MRE (cf. section LI-2: Reconstruction Error Analysis)

$$C^+_i = \max[0, x_i - (\mu_0 + K) + C^+_{i-1}] \quad \text{with} \quad C^+_0 = 0 \quad \text{and} \quad K = \frac{\delta}{2}\cdot\sigma^*_x \tag{16}$$

To evaluate the general suitability of the Cusum method for the leak identification problem, we created artificial error trajectories by adding different levels of white noise to given ground truth leak trajectories. This allowed us to confirm the algorithm's ability to robustly flag the leaks and to select the hyperparameters in a reasonable range (cf. Appendix). Moreover, we can derive some useful intuitions. Naturally, the change point method performs better for higher ratios of leak magnitude to signal noise. This reflects the fact that a smaller model error and better signal quality enable earlier leak detection. The same holds for the temporal development of the leak, as abrupt bursts are easier to detect than slow transients.

Leakage Localization

The leakage localization step has three subcomponents, including water demand calibration, pressure difference analysis to identify the pipes with the highest influence on the pressure sensors, and the application of the SLA method developed by Berglund et al. (2017) to quantify the approximate leakage magnitude and localize the leak in the WDN. The three steps shown in Fig. 1 work sequentially to, first, partially calibrate the hydraulic model using demand data. Second, a pressure difference analysis is conducted to define the order of the pipes that affect each pressure sensor of the water network and report them as leak candidates. Third, the application of SLA aims at finding the magnitude of a leak from the candidates that could be producing the discrepancy between nonleak and leak pressure values. A detailed explanation of each leak localization component is presented in what follows.

LL-1: Water Demand Calibration

Water demand calibration aims at matching the simulated and the observed demand to replicate real conditions with the hydraulic model (Walski 2017). LILA requires a demand-calibrated model to replicate the demand and the pressure measured values reported by the sensors. To calibrate the demand patterns and base demand in the WDN hydraulic model, we use automatic meter reading (AMR) data available for the simulation period. The new calibrated

Downloaded from ascelibrary.org by Andrea Cominola on 03/30/22. Copyright ASCE. For personal use only; all rights reserved.

demand patterns do not distinguish the type of user, e.g., residential or commercial, and overwrite the original demand patterns of the network with the new patterns obtained by normalizing the consumption reported by the AMR data, as shown in Eq. (17):

$$np = \frac{\sum_{t=1}^{N_{TS}} \frac{\sum_{j=1}^{N_{\text{AMR}}} d_{t,j}}{N_{\text{AMR}}}}{N_{TS}} \tag{17}$$

where np = average of new demand pattern; d = demand reported at time step t by AMR node j; N_{AMR} = number of AMR nodes; and N_{TS} = number of time steps. Hence, the output of this procedure is a hydraulic model with a period of simulation similar to that reported by AMR data and with simulated demand approximately matching the measured demand. Then the new base demand is calculated as follows:

$$bd_{\text{new}} = bd_{\text{orig}} \times \frac{\overline{d_{\text{meas}}}}{\overline{d_{\text{sim}}}} \tag{18}$$

where bd_{new} = new base demand of nonzero consumption nodes of network; bd_{orig} = original base demand of WDN hydraulic model; $\overline{d_{\text{sim}}}$ = mean of simulated demand calculated with new demand patterns; and $\overline{d_{\text{meas}}}$ = mean of measured demand reported by AMR nodes.

LL-2: Pressure Difference Analysis

A subset of pipes is identified for each MAS and considered as candidates to be evaluated by the SLA method described subsequently in LL-3. The pressure difference analysis evaluates the effect on sensors of a fixed-size leak inserted at each pipe of the network by comparing pressure values with and without the leak. Based on the anomalies between the leak and nonleak nodal pressure values modeled with hydraulic simulation, in Step LL-2 we define a pressure difference matrix (PDM), where each element $e_{i,j}$ is calculated as follows:

$$e_{i,j} = \sum_{t=1}^{N_{TS}} p^t_{\text{leak}_{i,j}} - p^t_{\text{noLeak}_{i,j}} \tag{19}$$

where $e_{i,j}$ represents the cumulative error between pressure with (p_{leak}) and without a leak (p_{noLeak}) from the sensor located at node i after a fixed-size leak is inserted on pipe j; p_{leak} and p_{noLeak} are obtained with hydraulic simulation, implemented in LILA using the Water Network Tool for Resilience (WNTR) Python package (Klise et al. 2018); and N_{TS} is the number of hydraulic time steps of the hydraulic model. The fixed leak used in this study corresponds to a flow of approximately 5% of the network's average flow, based on assumptions made in previously conducted research (Berglund et al. 2017; Kabaasha et al. 2020). This fixed-size leak corresponds to a flow rate of a background leak in the water network. The PDM is calculated once for the entire process, and its purpose is only to select the pipes affecting the most for each pressure sensor regardless of the number of simultaneous leaks. In the case of a significant mismatch between the estimated and the actual leak size, Step LL-3 described in what follows updates the final estimated leak magnitude. The simulation duration corresponds to the extended period of simulation (EPS) of the WDN hydraulic model, and pressure values are sampled at the end of the EPS to account for seasonality effects. The dimensions of the PDM are the number of pressure sensors as rows and the number of network pipes as columns. To identify the pipes that produce the highest effect on each pressure sensor after the fixed leak is inserted, we sort each row of PDM in descending order. We then include these pipes as candidate pipes for mathematical programming optimization to find the true leak location, described in the following section.

LL-3: Successive Linear Approximation

In the SLA step we formulate a simulation-optimization problem. The objective function, which is minimized, represents the absolute difference between observed and measured node pressure values, accounting for the effect of a leak on a set of candidate pipes. The leak magnitude is the decision variable. This procedure uses an iterative approach, and the magnitude of the leak is updated at each iteration while minimizing the error in pressure. The mathematical formulation of the minimization problem is presented in Eq. (20), followed by the definition of each term and the constraint on the decision variable. This formulation was adapted from the formulation provided by Berglund et al. (2017) as follows:

$$\begin{aligned}
&\min_x \|[A_{m\times n}][x_{n\times 1}] - [b_{n\times 1}]\| \\
&A_{m\times n} = \frac{p_{\text{leak}_i} - p_{\text{noLeak}_i}}{a_j} \\
&a_j = Q_j / p^{\alpha}_{\text{leak}_i} \\
&b = p_{obs_i} - p_{\text{noLeak}_i} \\
&\text{such that } x \geq 0
\end{aligned} \tag{20}$$

Each element in matrix A is the pressure response coefficient at pressure sensor $i \in \{1, \ldots, n\}$ for a leak with coefficient a_j simulated at pipe $j \in \{1, \ldots, m\}$. Leak coefficient a_j represents the relationship between the volumetric flow rate Q and the pressure p with the presence of a leak. a_j is initially assumed to be 1.0 to represent 1 m of pressure drop in the presence of a leak when using SI units and is updated in each step of the optimization. α is the pressure exponent and is assumed to be 0.5 (Crowl and Louvar 2001); p_{leak_i} is the simulated pressure in the presence of a leak retrieved from sensor i; p_{noLeak_i} is the simulated pressure without a leak; b is the independent term calculated as the difference between observed (p_{obs_i}) (e.g., from SCADA) and simulated pressure (p_{noLeak_i}), both at pressure sensor i; and x is the vector of leak coefficients obtained after optimization for the n candidate pipes using the m pressure sensors. In this work, we simulate a leak in a pipe by splitting the pipe and adding a leak on an additional temporary node located at the middle of the split pipe, as explained in the WNTR documentation (Klise et al. 2018). The number of candidate pipes included in the SLA analysis and selected from the LL-2 step depends on the characteristics of the hydraulic network and the layout of sensors. The method presented here can be applied for different hydraulic networks if the number of pressure sensors and the sampling times, as explained in what follows, prevent undetermined conditions when solving the expression $Ax = b$.

For improved performance, the application of SLA requires the start time of each leak, the MAS, and a list of the next most affected pressure sensors from the leakage identification step selected based on the signal strength reported from the sensors surrounding the MAS. SLA relies on the iterative application of linear programming (LP) and mixed integer linear programming (MILP) to solve the minimization problem shown in Eq. (20). LP and MILP use the L1 normalization procedure to determine the magnitude of a leak from the list of candidate pipes by minimizing the absolute difference between the simulated pressure under normal circumstances and the pressure after a leak is inserted at each candidate pipe. The localization step uses the start time of each event to insert a leak on each candidate pipe and sample the resulting pressure from the most affected pressure sensors. We sample pressure at several sampling times based on the following routine: first, a leak with

Downloaded from ascelibrary.org by Andrea Cominola on 03/30/22. Copyright ASCE. For personal use only; all rights reserved.

a coefficient (a) equal to 1.0 is inserted at the pipe connected to the MAS (Berglund et al. 2017). Second, the sampling times are defined as those where the simulated pressure without the leak is higher than the pressure with the leak, and the pressure values with the leak are close to the observed (i.e., measured) pressure values. This sampling time analysis aims to include more data points to compare observed and simulated pressure where the only discrepancy is due to the presence of a leak. Based on the sampled values, SLA solves an inverse problem of the form $Ax = b$, where the decision variable x represents the leak coefficients of each candidate pipe. The variable x is also referred to as the leak magnitude for given flow rate and pressure conditions. The initial optimization step uses LP to solve the $Ax = b$ expression, and the results are used to constrain the solution space for subsequent optimization steps, which apply the iterative LP and iterative MILP procedures. The output of the LL-3 subcomponent is the approximate leakage magnitude and the corresponding ID of the pipe that most likely contains the leak. When more than one magnitude is reported as greater than zero, the process selects the pipe with the highest impact on the MAS based on the pressure difference analysis (LL-2). The presence of more than one solution may be caused by other existing leaks, error in the model, or noise in pressure data.

Experimental Settings

Case Study

In this work, we apply LILA to the L-Town network and the data set provided by the organizing committee of BattLeDIM (Vrachimis et al. 2020a), a worldwide competition carried out in 2020 to assess and compare the results of various leak identification and localization methods submitted by participants. The L-Town network (Fig. 2) is a WDN based on an actual network located in Cyprus. It consists of 785 nodes, 905 pipes with a total length of 42 km, 1 pump, and 3 valves. The L-Town WDN is divided into three district metered areas (DMAs). DMAs A and B are directly connected to two water sources, i.e., reservoirs, whereas DMA C is connected to a tank that is filled up during night hours by a pump. L-Town is monitored through SCADA equipment, including flow rate meters at the exit of each reservoir, water level sensor of the tank, a set of 33 pressure sensors across the network, and a set of 82 AMR devices connected at the user level within DMA C.

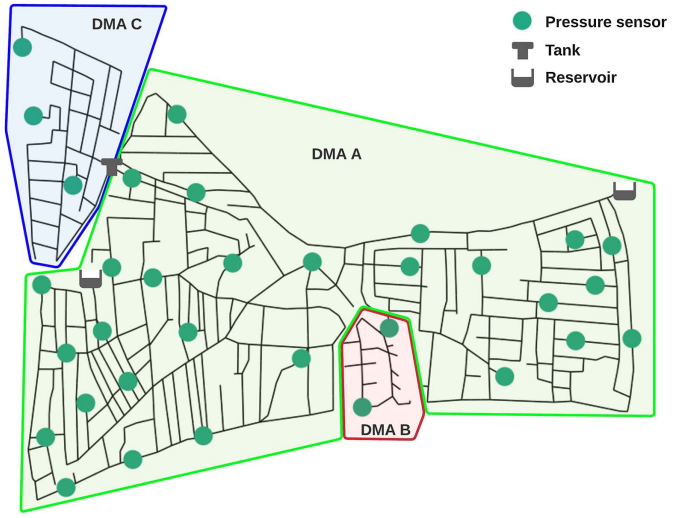

Fig. 2. Overview of L-town water distribution network, with highlighted pressure sensor locations.

Data from pressure sensors, AMR nodes, and flow meters located at the reservoirs and pump are reported by SCADA for 2018 and 2019 with a 5-min temporal resolution. SCADA data were simulated by the BattleDIM organizers using the WNTR hydraulic simulator (Klise et al. 2018). Moreover, noise was imposed on these data sets by modifying the pipe roughness and diameters to emulate differences between the hydraulic model and measured data and by adding white noise representing measurement noise.

The 2018 data were released prior to the competition and included pressure data from the 33 sensors, demand data from the 82 AMR meters, the water level of the tank, and the flow rate from reservoirs and the pump. Ground truth information for 10 leakages reported in 2018 was available and included the time when each leak was fixed and the corresponding pipe ID. The 2019 data set includes time series of the same variables observed in 2018, but no ground truth data were released prior to the BattLeDIM. Hence, here we consider ground truth information for the 2019 data set, which was released a posteriori, only as validation data to assess the performance of LILA. Over the 2-year period, 33 leaks were reported in total in L-Town. Besides the 10 reported leakages, 4 additional leaks occurred in 2018, yet they were not reported as part of the ground truth training data. These four leakages remained unfixed and, thus, continued in 2019. An additional 19 leakages started in 2019, summing up to a total of 23 leaks that were relevant for the evaluation of the BattLeDIM competition. The leaks are of two types, abrupt and incipient. Abrupt leaks are modeled as pipe bursts that occur suddenly, reaching their maximum magnitude instantly. Conversely, the magnitude of incipient leaks evolves gradually over time. A calibrated hydraulic model of the network for a week of simulation with 5-min hydraulic time steps was also provided. However, the model and the data have some discrepancies, as mentioned previously, owing to unknown conditions of the water system, including the actual status of pipes, roughness coefficients, and specific noise added to the data set by the BattLeDIM organizers [for more details, see Vrachimis and Eliades (2020)].

Performance Metrics

Leakage detection problems may be regarded as binary classification problems where the state with no leak and with leaks, respectively, represent the two classes of interest [cf. e.g., Taormina and Galelli (2018)]. The accuracy of a binary classifier used for anomaly detection can be assessed via the following four metrics: true positive (TP) and false positive (FP) indicating correct and incorrect classification of an anomalous state, respectively, and false negative (FN) and true negative (TN) indicating incorrect and correct classification of a normal state, respectively (Lever et al. 2016). Yet in the case of leakage detection, it is only partially of interest whether an individual data instance in time (e.g., the nodal pressure in a single time step) is classified as normal or anomalous, but rather the onset of the event that causes all subsequent anomalous states and its location constitute essential knowledge for the effective deployment of maintenance staff. To account for this, we assess LILA with an adapted version of the aforementioned metrics, as formulated by the BattLeDIM Committee (Vrachimis and Eliades 2020). The adopted definitions of TP, FP, FN, and TN report on the correct labeling of entire leaks regarding spatial and temporal occurrence rather than single instances in time. As such, TP and FN here denote the number of correct and missed leaks, respectively. Given the TTD of a leak, defined as the difference between its detection time t_d and its start time t_{start}

Downloaded from ascelibrary.org by Andrea Cominola on 03/30/22. Copyright ASCE. For personal use only; all rights reserved.

$$\text{TTD} = t_d - t_{\text{start}} \tag{21}$$

a reported leak is here considered TP if its estimated start time falls within its actual start and end times, t_{start} and t_{end} (i.e., the maximum allowed time to detection, $\text{TTD}_{\max}$, is positive and lower than the duration of the leak), and it is located within a maximum allowed pipe distance $u_{\max}$ from its true leak location. FN refers to a leak that is not detected at all by the method. FP is defined as a reported leak that is neither identified in time within the true leak lifespan nor localized within a distance $u_{\max}$ from its actual location. TN is set to zero since it is not applicable in the adapted formulation of the classification metrics. Because the threshold values $\text{TTD}_{\max}$ and $u_{\max}$ can be arbitrary, here we also analyze the sensitivity of the classification performance to varying threshold values.

Besides analyzing individual TP, FP, and FN metrics, we also compute the state-of-the-art classification metrics of *Recall*, *Precision*, and F_1-score. Recall measures the ability of a model to correctly identify anomalous instances in a data set. Precision measures the proportion of correctly identified anomalous instances compared to false alarms. Finally, the F_1-score is formulated as the weighted harmonic mean of Recall and Precision and varies between zero (worst performance) and one (best performance) (Lever et al. 2016)

$$\text{Recall} = \frac{\text{TP}}{\text{TP} + \text{FN}} \tag{22}$$

$$\text{Precision} = \frac{\text{TP}}{\text{TP} + \text{FP}} \tag{23}$$

$$F_1 = \frac{2 \times \text{Recall} \times \text{Precision}}{\text{Recall} + \text{Precision}} \tag{24}$$

In addition to the aforementioned classification metrics, we assess LILA by computing, for each leak, its TTD [Eq. (21) and Taormina et al. (2018)] and the volume of water leaked V_{leaked} from the start time of the leak t_{start} until the time of detection t_d

$$V_{\text{leaked}} = \int_{t_{\text{start}}}^{t_d} Q(\tau) d\tau \tag{25}$$

Finally, we compute the aggregate economic score S defined by the BattLeDIM organizers as

$$S = \sum_i p_w^i + c_r^i = \sum_i \left[\left(\int_{t_d^i}^{t_{\text{end}}^i} Q_j(\tau) d\tau \right) \times c_w - \min\left(\frac{u_{ij}}{u_{\max}}, 1 \right) c_R \right] \tag{26}$$

to account for the trade-off between the benefits p_w^i (i.e., NRW reduction) a water utility can obtain by the detection i of leakage j and the costs c_r^i for sending out a repair crew when an alarm is raised. The benefits p_w^i represent the opportunity cost for water saved from t_d to t_{end} considering leak flow Q_j and the cost for water c_w, which is set at €0.80/m^3. The repair cost c_r^i relates to the distance u_{ij} between the location of detection i and the actual position of leak j at a maximum fee c_R of €500 (Vrachimis and Eliades 2020).

Results

In this section, we present the numerical results obtained for leakage identification and localization by LILA on the L-Town data set introduced in the previous section. We compare the results obtained by LILA with the benchmark results obtained using an earlier version of the algorithm (hereafter called BattLeDIM benchmark), which we submitted for comparative assessment to the BattLeDIM competition (Daniel et al. 2020). LILA enhances the BattLeDIM benchmark with regard to both the identification and the localization modules. In the leakage identification step, the BattLeDIM benchmark does not include an automated change point detection step and relies on an expert-based annotation of the leak start time. LILA's identification step adds the automatic Cusum method. Furthermore, three improvements were incorporated in the leak localization step. First, the full set of pressure signals was considered for SLA optimization in the BattLeDIM benchmark, which added noise to the pressure difference. In LILA, only a limited set of sensors around the MAS are considered for each leak analysis. Second, to avoid the computational burden of analyzing dozens of candidate pipes, the BattLeDIM benchmark picked up to five candidate pipes spatially distributed around the MAS. Conversely, LILA uses up to 30 candidate pipes from the PDM for each leak event. This led to algorithm performance enhancement but also increased substantially the computational time. Third, while the BattLeDIM benchmark uses predefined sampling times for SLA, LILA searches for optimized sampling times for which the differences of observed data and simulated data including size-one leaks are minimized to account for time-variant noise. The demand-calibrated hydraulic model was the same used in the BattLeDIM and LILA versions.

In the following sections, we first present the overall score and performance assessment of LILA and compare it with the BattLeDIM benchmark. We then analyze in detail the results obtained for the leakage identification and leakage localization steps.

Overall LILA Performance Assessment

The performance metric results obtained for LILA and the BattLeDIM benchmark considering the threshold values $\text{TTD}_{\max} = \infty$ (indicating a maximum allowed TTD equal to the leak duration) and $u_{\max} = 300$ m defined in the BattLeDIM (Vrachimis and Eliades 2020) are reported in Table 1. LILA correctly identified and located 17 of the 19 leaks that started in 2019. All leaks were actually correctly identified, but two leaks were located outside of the search radius $u_{\max}$. This good performance is reflected in a Recall value of 1.0 and slightly lower Precision and F_1-score due to the inaccurate detection of two leaks. In terms of aggregate score S, LILA obtained a score of €307,852, outperforming the BattLeDIM benchmark, which obtained a total score of €191,055. All obtained classification metrics of LILA show a substantial improvement compared to the ones reported by the BattLeDIM benchmark. Note that both the BattLeDIM benchmark solution and the solution

Table 1. Performance metrics for LILA and BattLeDIM benchmark. The performance metrics are calculated using threshold values $\text{TTD}_{\max}$ equal to leak duration and $u_{\max} = 300$ m consistently with the settings of the BattLeDIM competition

Algorithm version	TP	FP	FN	Recall	Precision	F_1-score	S (€)
LILA	17	2	0	1.000	0.895	0.944	307,852
BattLeDIM benchmark	10	8	1	0.909	0.556	0.690	191,055

Downloaded from ascelibrary.org by Andrea Cominola on 03/30/22. Copyright ASCE. For personal use only; all rights reserved.

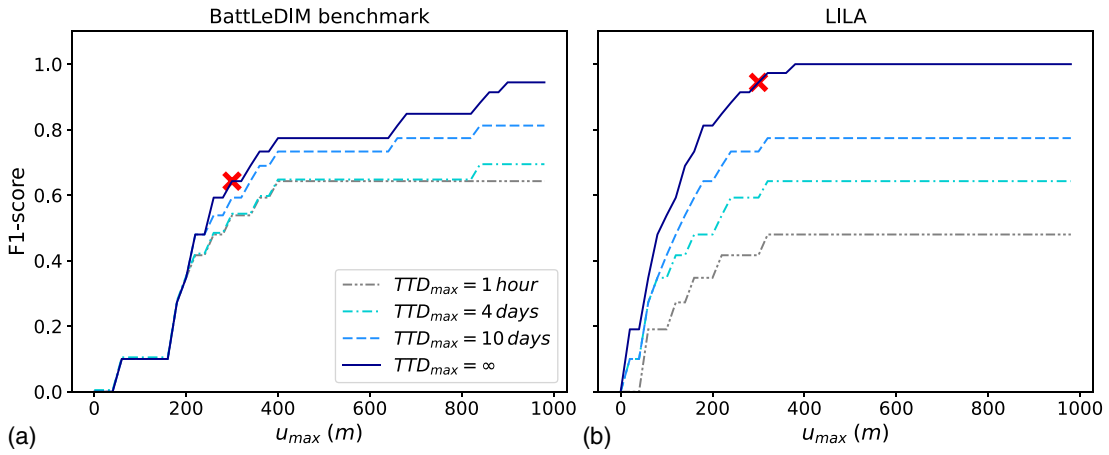

Fig. 3. F_1-score sensitivity to changing threshold parameters $u_{\max}$ and $\text{TTD}_{\max}$ for (a) BattLeDIM benchmark; and (b) LILA with Cusum change point annotation. The cross marker indicates the results obtained under default settings (Table 1).

obtained with LILA did not consider the four leaks that remained unfixed in 2018 by the L-Town utility and kept running during 2019 as only the 2019 data set was considered for algorithm testing in this work.

Sensitivity of LILA Performance to Classification Threshold Parameters

In addition to the foregoing performance assessment using default threshold values $\text{TTD}_{\max} = \infty$ and $u_{\max} = 300$ m, we evaluate the sensitivity of the F_1-score in response to changes in these two threshold parameters. Results are reported in Fig. 3.

The steeper incline of the curves reaching their maximum at lower $u_{\max}$ indicates that LILA performs better with respect to the distance between the estimated and actual leak location. This is reflected in the lower number of FPs for LILA as more detections fall within the respective permissible interval of $[0, u_{\max}]$. However, lower values of the F_1-score can be observed for a maximum permissible $\text{TTD}_{\max}$ of 1 h. This can be attributed to the difference in expert annotation of change points for the BattLeDIM benchmark compared to the automated Cusum annotation implemented in LILA. Most importantly, LILA achieves a perfect F_1-score of 1.0 for maximum permissible values of $\text{TTD}_{\max} = 41$ days and $u_{\max} = 374$ m. For these or any greater values of the two upper threshold parameters, LILA is capable of correctly identifying and localizing all leaks in the data set.

Detailed Assessment of Leakage Identification

Fig. 4 shows four exemplary leakage situations that occurred in the L-Town network across different time periods during 2019. For each leak, the signal of the ground truth leak flow Q_{leak} is compared to the MRE from the corresponding MAS. From this representation it is apparent that occurring leaks are directly reflected in the MRE since MRE rises with leak occurrence and diminishes again with leak repair. For instance, the start of the abrupt Leak 1 at Pipe p523 in Fig. 4(a) is not preceded by other leaks, resulting in low MRE values before and high values after its occurrence. With the onset of Leak 2 at Pipe p827, both MRE signals of n506 (closest to Leak 1) and n726 (closest to Leak 2) show an increase in magnitude compared to the situation with no leaks present, indicating that LILA is capable of detecting overlapping leaks. Incipient leaks are represented in the MRE in the same fashion, even reflecting the growth of the leak, as can be observed in Fig. 4(b). However, with the onset of abrupt Leak 6 at Pipe p514 during the growth process of Leak 4 at Pipe p653, the latter is temporarily obscured in this representation and only becomes visible again at a later stage. Similarly, the initial appearance of Leak 10 at Pipe p193 in Fig. 4(c) is obscured by the presence of both Leaks 7 and 8 at Pipes p331 and p142, respectively. For this and other similar instances, we analyzed individual trajectories of MRE_{ji} [cf. Eq. (13)] to obtain more precise start times. The complete set of all individual trajectories that were used for the subsequent change point detection is displayed in Fig. 5 and listed in Table 2.

A special case, represented in Fig. 4(d), arises in DMA C, where unknown irregular demand patterns are the cause of large noise in the MRE, obscuring individual leaks and making their identification more difficult. Hence, we chose to display the daily rolling mean instead of the raw MRE signal for better inspection. Nonetheless, LILA is able to identify both leaks occurring in DMA C by analyzing the raw MRE signal.

Moreover, Fig. 6 shows two exemplary MRE trajectories that were analyzed for change point detection (LI-3): on the left the abrupt Leak 1, on the right the incipient Leak 12. For both cases the signal-to-noise ratio enables a clear visual identification of the leak's development. Looking at the daily rolling means facilitates the visual inspection. It is worth noting that in the presence of either exemplary leak, further leaks started in different parts of the same DMA. Yet the trajectories enable making a clear distinction between overlapping leaks and are therefore well suited for the application of different change point detection methods. For a more detailed discussion on the effects of simultaneous leaks, we refer the reader to the "Discussion" section.

Fig. 7 compares the results of expert and Cusum change point annotation for abrupt [Figs. 7(a and c)] and incipient [Figs. 7(b and d)] leaks in terms of both TTD [Figs. 7(a and b)] and V_{leaked} [Figs. 7(c and d)]. The observation from Fig. 6 as to which abrupt leaks are detected much faster and more coherently than incipient leaks generalizes for all leaks and detection methods. The experts annotated most abrupt leaks on the spot with a maximum delay of 35 min (cf. Table 2). The LILA algorithm also flags most leaks immediately after occurrence and annotates all but one noteworthy exception within a maximum period of 2 h. The leak in Pipe 280 (leak ID 3), however, has such a challenging signal-to-noise ratio due to the strong irregular demand patterns in DMA C (cf. Fig. 5) that it is detected only after around 5 days (116 h). For incipient leaks, the average expert detection was approximately

Downloaded from ascelibrary.org by Andrea Cominola on 03/30/22. Copyright ASCE. For personal use only; all rights reserved.

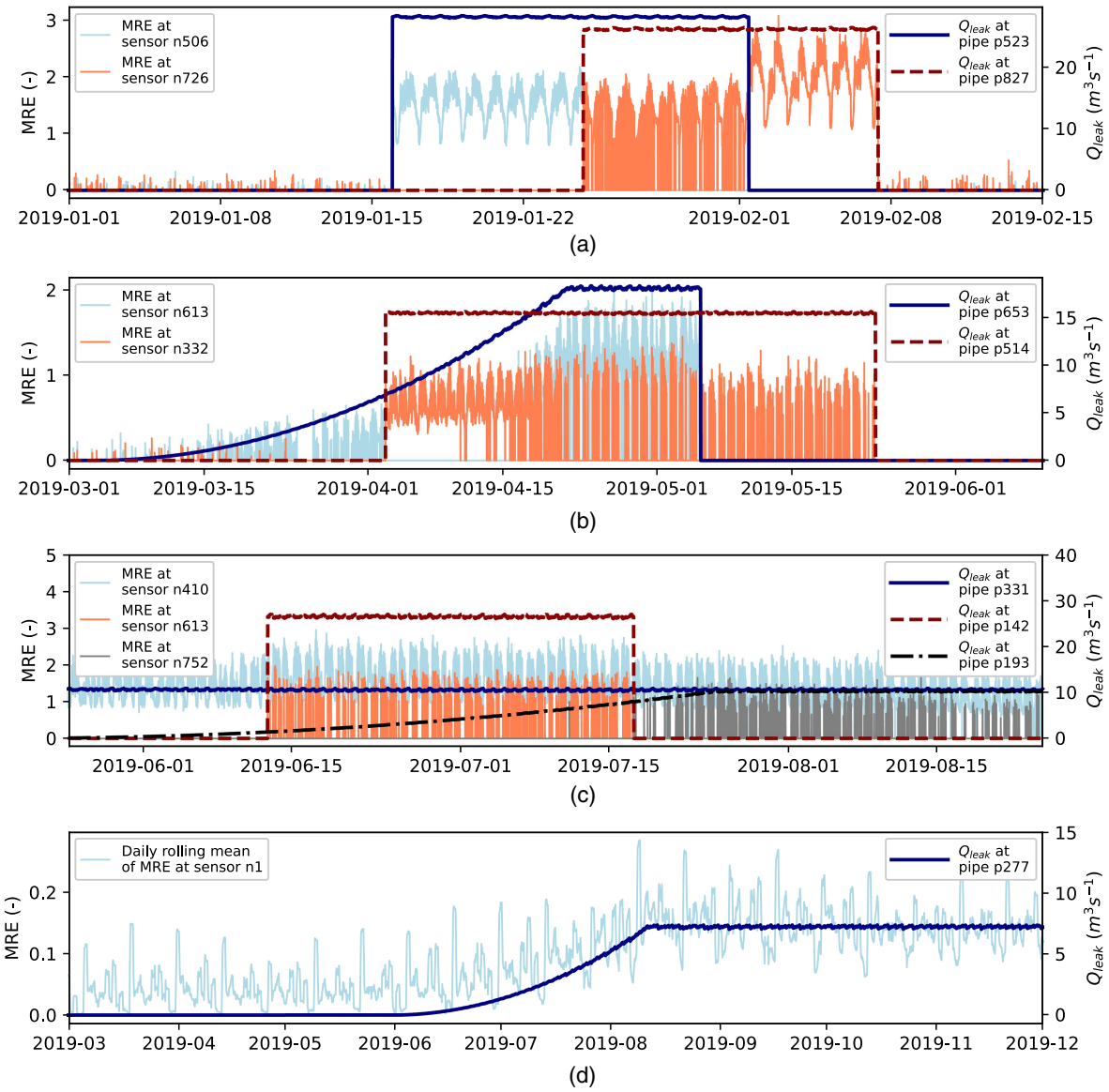

Fig. 4. Time series of MRE compared to ground truth data Q_{leak} for four different time windows: (a) overlapping of two abrupt leaks; (b) overlapping of abrupt leak during evolution of incipient leak; (c) occurrence of abrupt leak and an incipient leak in presence of another fully developed leak; and (d) evolution of incipient leak in DMA C with large noise caused by irregular demands.

7 days after the leak start, but two incipient leaks were actually missed by the expert (one annotated too early and one not at all), which highlights the uncertainty around manual annotations. The Cusum method, on the other hand, was slower in detecting incipient leaks with an average delay of around 20 days but annotated all existing leaks reliably. Overall, the defects translate to a total water savings of 402,562 m^3 for the expert and 440,338 m^3 for the Cusum method over the analyzed period of 1 year compared to no leak detection.

The fact that the experts were consistently faster than the Cusum method on the leaks they correctly identified is largely attributed to the asymmetry in information between the methods. The expert labeling was performed ex-post, in contrast to the online Cusum method. This implicit assumption of perfect foresight for the expert-based annotations makes the approach infeasible in practice. Furthermore, it would be impractical and nonscalable to manually monitor the system. Therefore, the Cusum method represents the baseline for an automated online application of the described methodology. However, the application of more advanced methods for automated leak detection might hold the potential to further improve the overall performance of the methodology in practice.

Detailed Assessment of Leakage Localization

The BattLeDIM benchmark only localized ten leaks at a distance lower than the threshold value $u_{\max} = 300$ m defined in the BattLeDIM (Table 3). Additionally, the localization step reports five leaks at distances greater than 600 m to the true leaking pipe. The poor performance shown by the initial localization step can be mainly attributed to the selection of the candidate pipes. As the SLA procedure assigns a leak to each candidate pipe and evaluates its effects on the sensors, it is computationally expensive when the list of candidate pipes contains 30 or more pipes for each event. To reduce the computational burden, we selected only five or six candidate pipes from the PDM in the BattLeDIM benchmark algorithm. The only condition we used to select these small sets of candidates for each event was that pipes had to be separated from each other by at least two pipes to ensure differences on the signal reported by the sensors due to the inserted leaks.

Downloaded from ascelibrary.org by Andrea Cominola on 03/30/22. Copyright ASCE. For personal use only; all rights reserved.

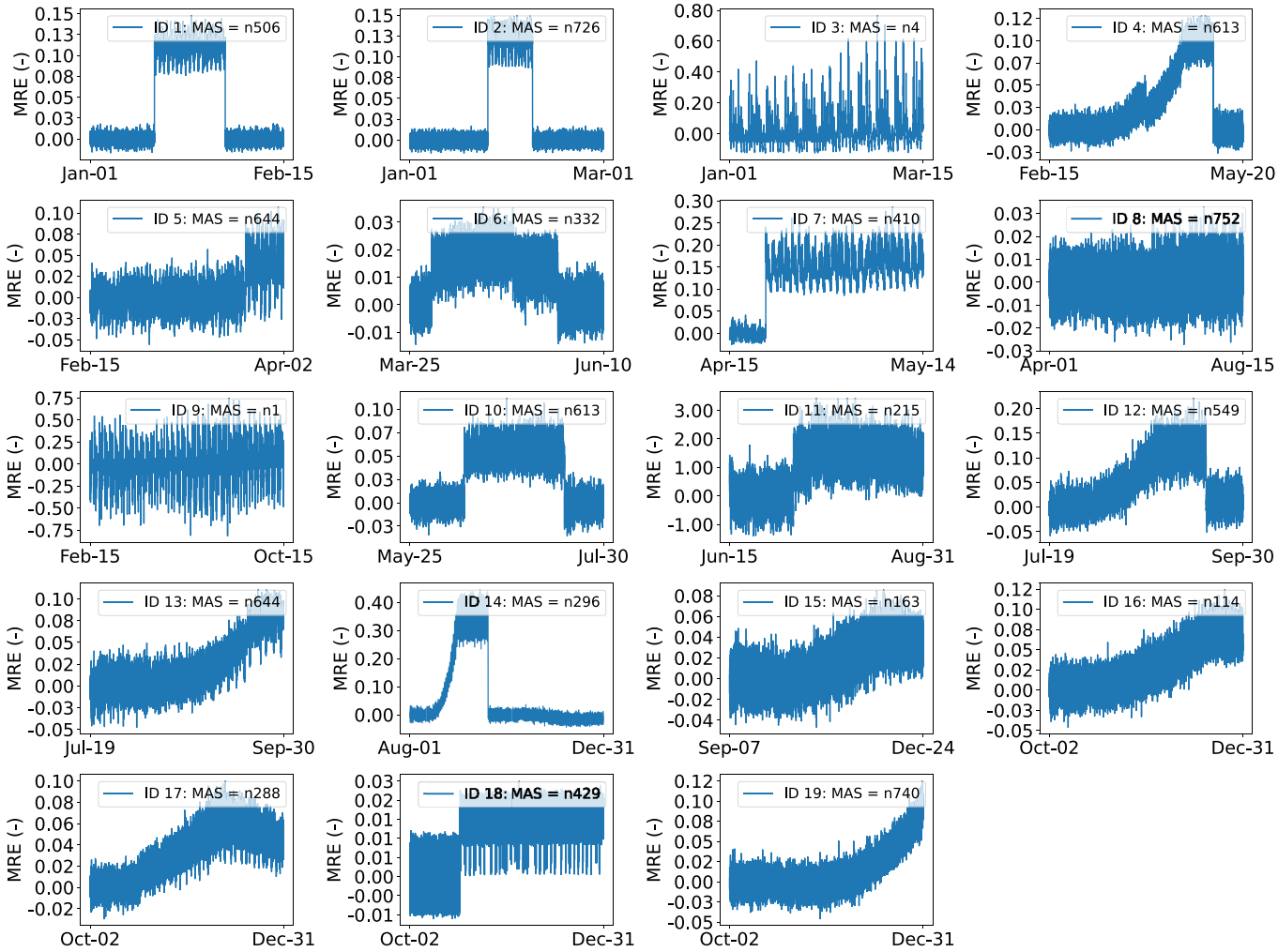

Fig. 5. Time series of *MRE* for each individual leak in DMA A on which change point detection was applied thereafter. The legend indicates the leak ID and its MAS.

Table 2. Performance comparison of leak identification methods (BattLeDIM benchmark versus LILA) applied to leaks in L-Town network in 2019

Leak properties			BattLeDIM benchmark		LILA	
ID	True start	Type	*TTD* (HH:mm)	V_{leaked} ($m^3\ s^{-1}$)	TTD (HH:mm)	V_{leaked} ($m^3\ s^{-1}$)
1	2019-01-15 23:00:00	Abrupt	00:00	0.0	00:00	0.0
2	2019-01-24 18:30:00	Abrupt	00:00	0.0	00:00	0.0
3	2019-02-10 13:05:00	Abrupt	00:35	3.0	116:10	603.5
4	2019-03-03 13:10:00	Incipient	166:50	20.2	222:30	47.9
5	2019-03-24 14:15:00	Abrupt	00:05	0.5	02:00	11.1
6	2019-04-02 20:40:00	Abrupt	00:00	0.0	00:10	2.6
7	2019-04-20 10:10:00	Abrupt	00:00	0.0	00:00	0.0
8	2019-05-19 10:40:00	Incipient	320:15	43.9	674:45	410.4
9	2019-05-30 21:55:00	Incipient	−262:05	28,875.9	1100:30	1,057.2
10	2019-06-12 19:55:00	Abrupt	00:00	0.0	00:00	0.0
11	2019-07-10 08:45:00	Abrupt	00:00	0.0	01:05	5.8
12	2019-07-26 14:40:00	Incipient	129:50	24.1	272:00	221.4
13	2019-08-02 03:00:00	Incipient	400:00	177.4	274:00	57.0
14	2019-08-16 14:00:00	Incipient	65:40	7.2	116:30	40.3
15	2019-09-13 20:05:00	Incipient	not detected	12,505.9	974:05	815.4
16	2019-10-03 14:00:00	Incipient	274:00	24.1	748:05	490.0
17	2019-10-09 10:15:00	Incipient	295:45	78.1	387:15	175.4
18	2019-10-25 13:25:00	Abrupt	00:15	3.3	00:15	3.3
19	2019-11-20 11:55:00	Incipient	108:05	4.6	44:15	0.3

Note: This table is organized chronologically by the true start time of the leak, also indicating whether a leak occurred abruptly or in an incipient fashion. The TTD and water volume leaked until detection, V_{leaked}, are presented for both the BattLeDIM benchmark and the LILA algorithm.

Downloaded from ascelibrary.org by Andrea Cominola on 03/30/22. Copyright ASCE. For personal use only; all rights reserved.

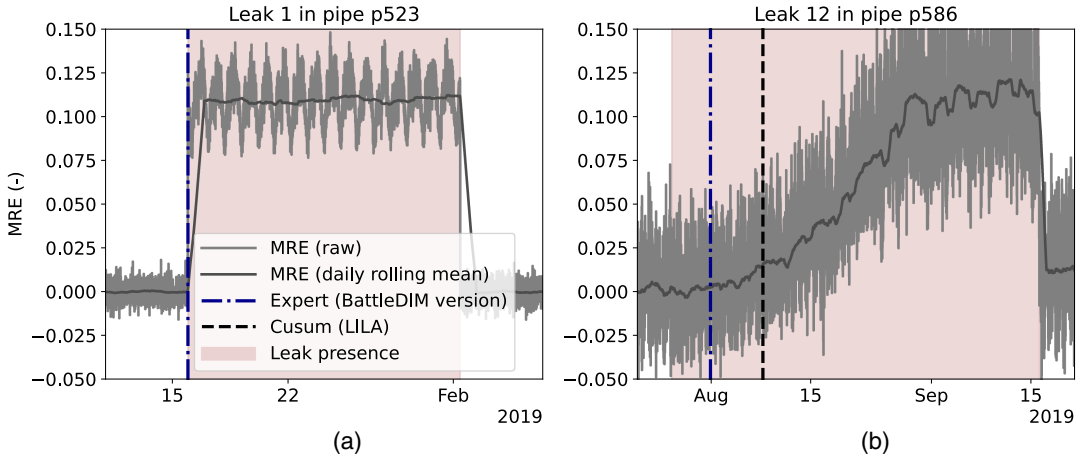

Fig. 6. Exemplary MRE trajectories during leakages and their respective annotations by expert and Cusum method. (a) Leak 1 (abrupt); and (b) Leak 12 (incipient).

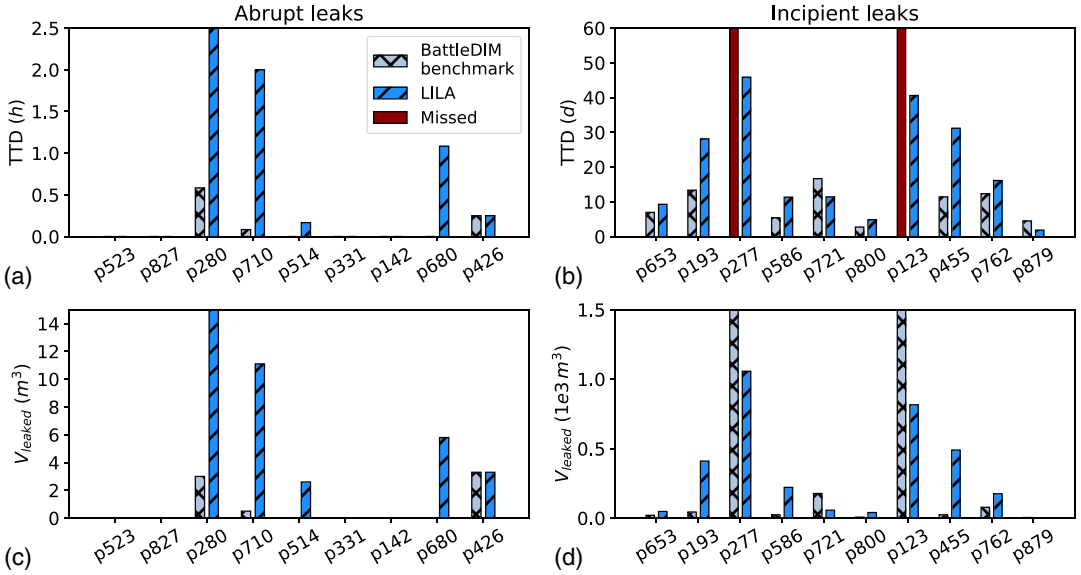

Fig. 7. Comparison of expert and Cusum leak annotation: (a, b) time to detection; and (c, d) leaked water volume. Results are reported for abrupt (a, c) and incipient (b, d) leaks. No bars indicate no detection delay or no water loss. The *y*-axis range in (a) is limited to [0,25] hours for visualization purposes, but the leak located in pipe p280 was detected by LILA with a delay of 116 h and 10 min (see Table 2).

In this work, we present the capability of the enhanced identification-localization method LILA, which includes the analysis of all top 30 pipes from the PDM as candidates for each event in the localization step. Furthermore, for each leak, we only used the MAS combined with three to five additional sensors to avoid extra noise that might be introduced by sensors not affected by some spatially distant leaks. Each additional sensor was selected for each event based on signal strength. Depending only on the signal and not on topological or geographical conditions, some leaks were analyzed with three and others with up to five sensors in addition to the MAS. Fig. 8 displays the effect of this adaption by comparing the BattLeDIM benchmark and the LILA algorithms.

LILA finds leaks with an average search radius of 149 m. Of the 19 leaks localized during 2019, 37% was within a 100-m radius, 53% of leaks had a distance ranging from 100 and 300 m from the true leaking pipe, and 10% were located outside of the maximum allowable distance of 300 m used in the BattLeDIM competition. There are two events where the localization step found the exact location, Leaks 8 and 19, whereas Leak 9 was the event reported by LILA with the maximum distance from the true location (374 m) (Fig. 9). The localization step does not differentiate between incipient and abrupt leaks; however, owing to the multiple sample times to retrieve pressure values, SLA reports slightly better performance for the incipient leaks compared to abrupt leaks. While LILA outperforms the BattLeDIM benchmark, there are events where the localization step does not improve the location reported by the BattLeDIM benchmark because of the noise in the data and the difference between the detected and the true start time of the leaks. SLA depends on a well-calibrated pressure model reporting values close enough to the values reported by SCADA. When there is substantial error between the measured and simulated pressures, the performance of the SLA approach is significantly affected.

Downloaded from ascelibrary.org by Andrea Cominola on 03/30/22. Copyright ASCE. For personal use only; all rights reserved.

Table 3. Performance comparison of localization methodology (BattLeDIM benchmark versus enhanced, selective version LILA) applied to L-Town network for leaks of 2019. The order of this table follows the organization in Table 2

Leak properties		BattLeDIM benchmark		LILA		
ID	True location	Detected location	Distance (m)	Detected location	Sensors considered for SLA	Distance (m)
1	p523	p114	166	p498	n506, n105, n114, n469, n516	54
2	p827	p845	295	p823	n726, n752, n722, n769, n740	203
3	p280	p30	255	p283	n1, n4, n31	124
4	p653	p664	324	p647	n613, n188, n163, n342, n458	93
5	p710	p80	178	p703	n644, n288, n679, n769	221
6	p514	p87	212	p513	n332, n495, n506, n105, n469	51
7	p331	p322	391	p391	n410, n54, n429	103
8	p193	p58	890	p193	n752, n769, n740	0
9	p277	p247	147	p267	n1, n4, n31	374
10	p142	p644	343	p657	n613, n188, n163, n342, n458	304
11	p680	p737	187	p76	n215, n229	66
12	p586	p204	205	p135	n549, n516, n188, n519	169
13	p721	p153	253	p705	n644	294
14	p800	p692	823	p174	n296, n722, n740, n726, n769	167
15	p123	Not detected		p127	n163 n519 n458	76
16	p455	p587	858	p452	n114, n105, n469, n516, n495	136
17	p762	p79	668	p785	n288, n752, n726, n679, n769	258
18	p426	p425	50	p893	n429, n54, n410, n342, n458	144
19	p879	p885	643	p879	n740, n769, n296, n722, n752, n726	0

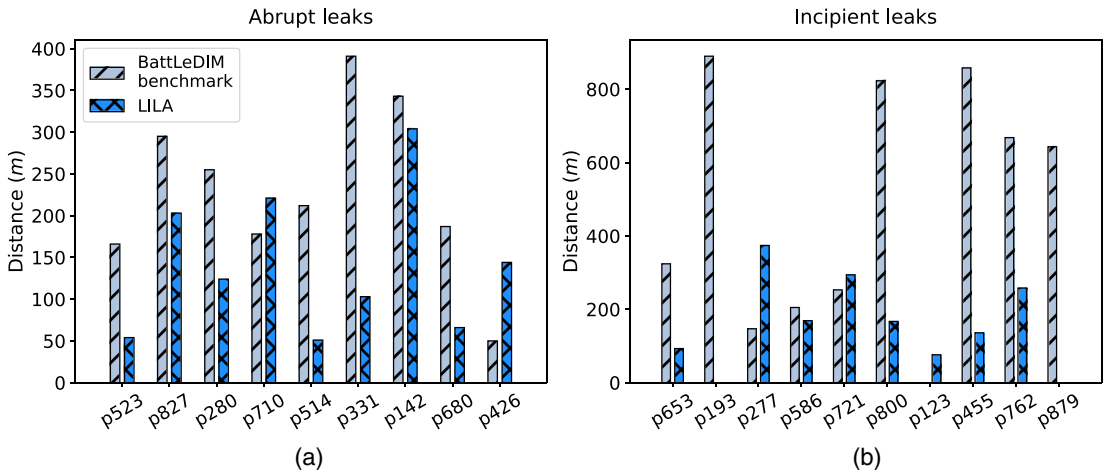

Fig. 8. Distances of identified leaking pipes to true leak location for (a) abrupt; and (b) incipient leaks.

Discussion

The numerical results we obtained by testing LILA on data from the L-Town WDN case study overall demonstrated its suitability to perform leakage identification and localization based on pressure data with high temporal resolution. Almost all ground truth leakages were promptly identified and were localized within an acceptable distance from the actual location. Yet the following specific methodological aspects of the leakage identification and leakage localization phases in LILA require further investigation to make it of general value and ultimately usable for complex real-world applications.

First, as mentioned in the "Methods" section, the current version of the proposed LILA algorithm is not able to automatically identify leaks that occur in DMAs where unknown, irregular demand patterns are present (i.e., as in DMA C of the L-Town WDN). When irregular demand patterns are known, e.g., pump operation in the L-Town WDN, they may be included in the regression model used for leakage identification and, hence, pose no problem to the method. Yet, unknown irregular demand patterns cannot be easily included in the model, leading to higher residual error of the regression model and hindering the analysis of leakages. If LILA were coupled with a method capable of learning unknown demand patterns from the available data, it would become suitable for analysis on any WDN, regardless of the characteristics of its demand patterns.

Another important factor in the successful application of the identification phase of LILA is the availability of a time period in the absence of newly occurring leaks or other similar transient effects for training or calibration purposes. Within this work, we selected the training period manually based on preliminary data exploration and visualization to obtain low values of the model residual for this period. Because the regression model for leakage identification [Eq. (12)] may have to be recalibrated after the occurrence of a new leak or due to changing demand, a manual approach may be impractical for real-world applications. A more scalable version of LILA would require an automatic selection of an optimal subset of data for training.

Downloaded from ascelibrary.org by Andrea Cominola on 03/30/22. Copyright ASCE. For personal use only; all rights reserved.

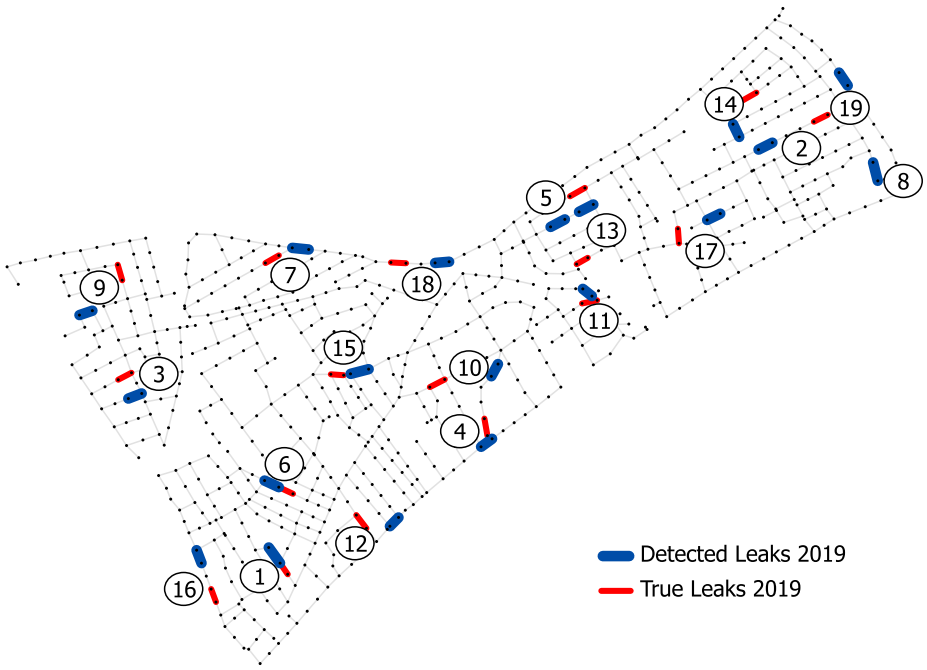

Fig. 9. True and detected leaks that started in 2019 using LILA. Circled numbers represent event number as shown in Table 3.

Third, unlike the BattLeDIM benchmark, the leakage identification phase in LILA incorporates automated change point detection. We implemented an online change point detection method (see "Methods" section) to make LILA more suitable for an application within a real-world setting, compared to the expert-based estimation of leak start times of the BattLeDIM version. However, the numerical results we obtained using the online change point detection method revealed a significant drawback regarding the TTD in comparison with the expert-based annotation used in the BattLeDIM benchmark. It is worth noting that the expert-based annotations were made ex-post, rather corresponding to an offline fashion of change point detection. This consideration opens up the need for a more systematic analysis to compare the performance of different offline and online change point detection methods for the analysis of the residual error produced by the leakage identification regression model. While online change point detection may entail quicker availability of the results, i.e., alarms are raised more promptly, the application of offline detection methods with a limited time horizon may also be accurate and lead to timely identification of leaks. The choice of an optimal change point detection method should therefore not be limited to either online or offline capabilities, but it is rather the solution of a multicriteria problem that considers the trade-offs between TTD, effort needed for calibration, ease of implementation, and low susceptibility to false alarms.

Another factor that needs further investigation is the method's sensitivity to leaks that occur in temporal and spatial proximity. The method presented here was able to distinguish between multiple parallel leaks that occurred in the BattleDIM data sets, but we have no information about the capabilities or limitations of the method in identifying parallel leaks for other data sets. Further research can involve experiments that vary spatial and temporal distances between leaks to explore the method's boundaries. We expect that the results will depend on the availability and placement of sensing equipment in the network, which is another interesting subject for further research.

Finally, the SLA used in the leakage localization phase relies on an almost error-free model, where the only disturbance between the measured and simulated pressure is due to an unusual event. However, an error-free model is rarely available. The error induced by the actual status of the network components and the noise of the measured data prevent SLA from accurately identifying the true leaking pipe. To partially address this issue, we modified the demand patterns and the base demand of the hydraulic model to improve the match between the simulated and measured data across the network. However, the new demand patterns do not distinguish the type of user, residential or commercial, and overwrite the original demand patterns of the network with the new patterns. Hence, alternative ways to mitigate the effect of model errors need further investigation. Correction of model error can leverage the combination of identification and localization to provide a reliable set of leaks in research studies and practical applications (van Thienen 2021).

Conclusions

In this paper we developed and described LILA, a pressure-driven algorithm for leakage identification and localization in WDNs. We developed LILA within the scope of the BattleDIM (Vrachimis et al. 2020a), where we submitted the results from an early version of the algorithm (Daniel et al. 2020).

LILA includes a sequential two-step procedure composed of a leakage identification module and a leakage localization module. The leakage identification module detects the presence of a leak, estimates its starting time, and pinpoints the pressure sensor that is most affected by the leak (called MAS in this paper). The leakage localization module uses the information provided by the identification step and a calibrated hydraulic model to estimate the location of the identified leakages. First, a leak is simulated on a set of candidate pipes. Then successive linear approximation is applied to find the location and magnitude of the leak by minimizing the difference between measured and simulated pressure values. Compared to its initial version introduced in Daniel et al. (2020), we refined LILA with the inclusion of more candidate pipes for leakage localization and by restricting the search using only the MAS for

Downloaded from ascelibrary.org by Andrea Cominola on 03/30/22. Copyright ASCE. For personal use only; all rights reserved.

each event, which improved the computational burden of the simulation-optimization method used in leakage localization.

We tested the ability of LILA to solve the challenge of finding a set of leaks occurring during 2019 in the L-Town WDN, a virtual representation of a real water network in Cyprus, created for the BattLeDIM (Vrachimis et al. 2020a). In light of the numerical results we obtained by assessing the performance of LILA with multiple performance metrics based on leak classification accuracy, estimation accuracy of the leak start time and location, and an aggregate monetary score, we assert that LILA can accurately identify and localize leakages occurring in WDNs monitored with a distributed network of pressure sensors collecting data with high resolution (5-min temporal resolution in this work). The initial version of our algorithm presented as part of the BattLeDIM by our Leakbusters team (Daniel et al. 2020) and used in this paper as a benchmark achieved a score of €191,055 and was ranked third by the BattLeDIM organizers, out of 18 participating teams worldwide. The improved version presented in this paper with the name "LILA" achieved a total economic score of €307,852, which outperforms economically the score of €260,562 obtained by the winning team of the BattLeDIM (Vrachimis and Eliades 2020). Finally, this enhancement in performance comes at a computational cost. While the BattLeDIM version used 5 candidate pipes selected based on geographical proximity to the MAS, LILA uses up to 30 candidate pipes selected based on the pressure difference analysis described in section LL-2: Pressure Difference Analysis and increased the running time by over 20 times for each leak.

Detailed results showed that LILA identified all 19 considered leaks, with an overall F_1-score exceeding 0.94 considering the threshold values of the BattLeDIM and could obtain an F_1-score of 1.0 for maximum permissible distances of $u_{\max} = 374$ m. Abrupt leakages were identified immediately or with little delay, usually less than 2 h, while up to 20 days were required on average by automatic change point detection to raise alarms on incipient leakages. Finally, LILA could localize leaks within an average distance of 149 m from the true leaking pipe. These results are promising in terms of moving forward with the development of leakage detection algorithms capable of exploiting the increasing amount of online sensor-based information gathered and transmitted by pressure sensors distributed in WDNs.

Overall, the contributions and limitations of this work offer several opportunities for further research, primarily related to making LILA of general use and applicability in real-world settings. First, we acknowledge that the prompt identification of incipient leaks remains a challenge for many change point detection methods, so more comparative analyses and investigations would be needed to improve its identification performance without resulting in an increase in the FP rate. Second, model-based leakage localization is sensitive to model errors. While LILA was able to localize leakages with an average distance of 149 m in the case study presented in this paper, the requirement of an almost error-free pressure-calibrated model would cause a dramatic decrease in localization performance with models available in most real-world cases. Moreover, the selection of the candidate pipes can still be, also in the refined version of LILA, a computationally expensive procedure because it relies on simulating a leak at every single pipe of the system and measuring its impact on the pressure sensors installed across the system. Finally, irregular water demand should be modeled and incorporated into LILA and stress tests with real-time SCADA data and benchmarking in real-world applications would make it suitable for use in practice.

More benchmark data sets and testing platforms similar to the BattLeDIM and structured collaborative work with water utilities willing to leverage their ongoing digitalization efforts with integrated data-driven analytics would enable further development and testing of methods like LILA with the ultimate goal of addressing the aforementioned open challenges and ultimately making them suitable and fully reliable for inclusion in utilities' leakage management operations.

Appendix. Choice of Hyperparameters for the Cusum Change Point Detection Method

The Cusum method requires an estimate of the signal standard deviation, a choice of δ, and a threshold parameter $H = \eta \times \sigma_x$, which itself is related to the choice of δ [cf. Eq. (16)]. To assess the algorithm's ability to robustly flag the leaks and to select the hyperparameters in a reasonable range, we first applied the Cusum method in a controlled environment. Since leak size correlates with

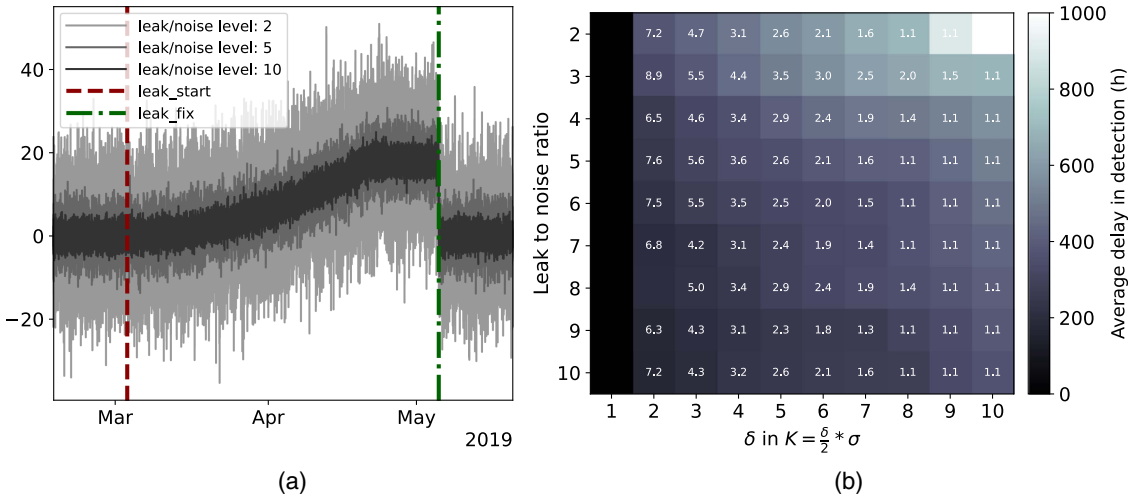

Fig. 10. (a) Exemplary transient leak error trajectory for different noise levels (a *leak/noise* level of 2 corresponds to Gaussian noise with standard deviation of half the maximum leak magnitude); and (b) overview Cusum-hyperparameter search. The heatmap color indicates the average detection delay, and numbers represent optimal threshold levels η. Configurations without optimal threshold levels did not produce a result without false positives and were therefore neglected.

Downloaded from ascelibrary.org by Andrea Cominola on 03/30/22. Copyright ASCE. For personal use only; all rights reserved.

pressure drops and therefore with the MRE development, we took the leak water loss trajectories (ground truth) and added random noise to get a realistic estimate of the MRE structure [Fig. 10(a)]. We then applied the algorithm for various configurations of δ and η. The results are displayed in Fig. 10(b).

In practice, the MRE standard deviation can be estimated over the calibration period with no leak. Moreover, it was empirically found that a suitable combination of the hyperparameters for the Cusum method are $\delta = 4$ and $\eta = 3$, which is indeed close to the theoretical results. However, in DMA C, these settings needed to be adjusted because of the irregular demand patterns' impact on the MRE. There, we used a δ of 1 and $\eta = 300$ to account for the strong patterns in the MRE time series.

Data Availability Statement

Some or all data, models, or code generated or used during the study are available in online repositories in accordance with funder data retention policies (Vrachimis et al. 2020b; Daniel et al. 2021; Pesantez 2021). Some or all data, models, or code that support the findings of this study are available from the corresponding author upon reasonable request.

Acknowledgments

The authors would like to thank the BattLeDIM Committee for organizing and managing the BattLeDIM competition and for coordinating and guest editing this special collection. Moreover, the authors acknowledge the support of HEIBRiDS. JP would like to acknowledge the Government of Ecuador for its funding. This material is based on work that was partially supported by the US National Science Foundation's Division of Industrial Innovation and Partnerships under Grant PFI-1919228.

Notation

The following symbols are used in this paper:

A = sensitivity matrix used in Step LL-3;
$\mathcal{A}$ = area;
a = leak coefficient;
b = vector of pressure differences;
bd_{new} = new base demand;
bd_{orig} = original base demand;
C = Cusum parameter;
c = cost;
D = set of demand patterns;
d = demand;
$E(\cdot)$ = expectation operator;
e = matrix element of PDM;
F = set of all pipes in corresponding flow path;
fr = frictional loss indicator;
g = gravitational constant;
H = Cusum threshold parameter;
h = hydraulic head;
i, j = node indicators;
K = Cusum correction factor;
k = regression coefficient;
L = set of all leakages in water distribution network;
l = leak indicator;
m = minor loss indicator;
N_{AMR} = number of automatic meter reading nodes;
N_{TS} = number of time steps;
np = vector of new demand patterns;
P = pressure;
p = pipe indicator;
p_w = score from saved nonrevenue water;
Q = volumetric flow rate;
S = economic score;
s = most affected sensor;
t = time;
u = leak location distance measure;
V = volume;
v = velocity;
Z = geodetic height;
α = pressure exponent;
γ = specific weight;
δ = Cusum control parameter;
η = Cusum specific threshold;
μ = mean; and
σ = standard deviation.

References

Aminikhanghahi, S., and D. J. Cook. 2017. "A survey of methods for time series change point detection." *Knowl. Inf. Syst.* 51 (2): 339–367. https://doi.org/10.1007/s10115-016-0987-z.

Arregui, F. J., R. Cobacho, J. Soriano, and R. Jimenez-Redal. 2018. "Calculation proposal for the economic level of apparent losses (ELAL) in a water supply system." *Water* 10 (12): 1809. https://doi.org/10.3390/w10121809.

Atef, A., T. Zayed, A. Hawari, M. Khader, and O. Moselhi. 2016. "Multi-tier method using infrared photography and GPR to detect and locate water leaks." *Autom. Constr.* 61 (Jan): 162–170. https://doi.org/10.1016/j.autcon.2015.10.006.

AWWA (American Water Works Association). 2008. Vol. 36 of *Water audits and loss control programs*. Denver, CO: AWWA.

Berglund, A., V. S. Areti, D. Brill, and G. Mahinthakumar. 2017. "Successive linear approximation methods for leak detection in water distribution systems." *J. Water Resour. Plann. Manage.* 143 (8): 04017042. https://doi.org/10.1061/(ASCE)WR.1943-5452.0000784.

Beuken, R., C. Lavooy, A. Bosch, and P. Schaap. 2008. "Low leakage in the Netherlands confirmed." In *Proc., 8th Water Distribution Systems Analysis Symp. 2006*, 1–8. Reston, VA: ASCE. https://doi.org/10.1061/40941(247)174.

Bohorquez, J., B. Alexander, A. R. Simpson, and M. F. Lambert. 2020. "Leak detection and topology identification in pipelines using fluid transients and artificial neural networks." *J. Water Resour. Plann. Manage.* 146 (6): 04020040. https://doi.org/10.1061/(ASCE)WR.1943-5452.0001187.

Cominola, A., E. Spang, M. Giuliani, A. Castelletti, J. Lund, and F. Loge. 2018. "Segmentation analysis of residential water-electricity demand for customized demand-side management programs." *J. Cleaner Prod.* 172 (Jan): 1607–1619. https://doi.org/10.1016/j.jclepro.2017.10.203.

Covas, D., and H. Ramos. 2010. "Case studies of leak detection and location in water pipe systems by inverse transient analysis." *J. Water Resour. Plann. Manage.* 136 (2): 248–257. https://doi.org/10.1061/(ASCE)0733-9496(2010)136:2(248).

Crowl, D. A., and J. F. Louvar. 2001. *Chemical process safety: Fundamentals with applications*. Boston: Pearson Education.

Daniel, I., S. Letzgus, and A. Cominola. 2021. "LILA (Code)." Accessed December 15, 2021. https://github.com/SWN-group-at-TU-Berlin/LILA.

Daniel, I., J. Pesantez, S. Let, M. A. Khaksar Fasaee, F. Alghamdi, K. Mahinthakumar, E. Berglund, and A. Cominola. 2020. "A high-resolution pressure-driven method for leakage identification and

Downloaded from ascelibrary.org by Andrea Cominola on 03/30/22. Copyright ASCE. For personal use only; all rights reserved.

localization in water distribution networks." Accessed March 15, 2021. https://doi.org/10.5281/zenodo.3924632.
Fang, Q., J. Zhang, C. Xie, and Y. Yang. 2019. "Detection of multiple leakage points in water distribution networks based on convolutional neural networks." *Water Supply* 19 (8): 2231–2239. https://doi.org/10.2166/ws.2019.105.
Golub, G. H., and C. F. Van Loan. 2013. *Matrix computations*. 4th ed. Baltimore: The Johns Hopkins University Press.
Guo, G., X. Yu, S. Liu, Z. Ma, Y. Wu, X. Xu, X. Wang, K. Smith, and X. Wu. 2021. "Leakage detection in water distribution systems based on time-frequency convolutional neural network." *J. Water Resour. Plann. Manage.* 147 (2): 04020101. https://doi.org/10.1061/(ASCE)WR.1943-5452.0001317.
Kabaasha, A., J. van Zyl, and G. Mahinthakumar. 2020. "Correcting power leakage equation for improved leakage modeling and detection." *J. Water Resour. Plann. Manage.* 146 (3): 06020001. https://doi.org/10.1061/(ASCE)WR.1943-5452.0001172.
Kazeminasab, S., V. Janfaza, M. Razavi, and M. K. Banks. 2021. "Smart navigation for an in-pipe robot through multi-phase motion control and particle filtering method." Preprint submitted February 23, 2021. http://arxiv.org/abs/2102.11434.
Klise, K., R. Murray, and T. Haxton. 2018. "An overview of the water network tool for resilience (WNTR)." In Vol. 1 of *Proc., 1st Int. WDSA/CCWI Joint Conf.* Reston, VA: ASCE.
Lever, J., M. Krzywinski, and N. Altman. 2016. "Classification evaluation." *Nat. Methods* 13 (8): 603–604. https://doi.org/10.1038/nmeth.3945.
Levinas, D., G. Perelman, and A. Ostfeld. 2021. "Water leak localization using high-resolution pressure sensors." *Water* 13 (5): 591. https://doi.org/10.3390/w13050591.
Liemberger, R., and P. Marin. 2006. *The challenge of reducing non-revenue water in developing countries-how the private sector can help: A look at performance-based service contracting*. Washington, DC: World Bank.
Makropoulos, C., and D. Savic. 2019. "Urban hydroinformatics: Past, present and future." *Water* 11 (10): 1959. https://doi.org/10.3390/w11101959.
Mansour-Rezaei, S., G. Naser, A. Malekpour, and B. W. Karney. 2013. "Contaminant intrusion in water distribution systems." *J. Am. Water Works Assn.* 105 (6): E278–E290. https://doi.org/10.5942/jawwa.2013.105.0061.
Misiunas, D., J. Vftkovsky, G. Olsson, M. Lambert, and A. Simpson. 2006. "Failure monitoring in water distribution networks." *Water Sci. Technol.* 53 (4–5): 503–511. https://doi.org/10.2166/wst.2006.154.
Misiunas, D., J. Vftkovsky, G. Olsson, A. Simpson, and M. Lambert. 2005. "Pipeline break detection using pressure transient monitoring." *J. Water Resour. Plann. Manage.* 131 (4): 316–325. https://doi.org/10.1061/(ASCE)0733-9496(2005)131:4(316).
Montgomery, D. C. 2020. *Introduction to statistical quality control*. 8th ed. Hoboken, NJ: Wiley.
Morris, R., Jr. 1967. "Principal causes and remedies of water main breaks." *J. Am. Water Works Assn.* 59 (7): 782–798. https://doi.org/10.1002/j.1551-8833.1967.tb03414.x.
Perez, R., V. Puig, J. Pascual, A. Peralta, E. Landeros, and L. Jordanas. 2009. "Pressure sensor distribution for leak detection in Barcelona water distribution network." *Water Sci. Technol. Water Supply* 9 (6): 715–721. https://doi.org/10.2166/ws.2009.372.
Pesantez, J. 2021. "LeakLocalization (Code)." Accessed December 15, 2021. https://github.com/jorgeps86/LeakLocalization.
Puust, R., Z. Kapelan, D. Savic, and T. Koppel. 2010. "A review of methods for leakage management in pipe networks." *Urban Water J.* 7 (1): 25–45. https://doi.org/10.1080/15730621003610878.
Sarni, W., C. White, R. Webb, K. Cross, and R. Glotzbach. 2019. *Digital water: Industry leaders chart the transformation journey.* London: International Water Association and Xylem.
Soldevila, A., R. M. Fernandez-Canti, J. Blesa, S. Tornil-Sin, and V. Puig. 2017. "Leak localization in water distribution networks using Bayesian classifiers." *J. Process Control* 55 (Jul): 1–9. https://doi.org/10.1016/j.jprocont.2017.03.015.
Sophocleous, S., D. Savić, and Z. Kapelan. 2019. "Leak localization in a real water distribution network based on search-space reduction." *J. Water Resour. Plann. Manage.* 145 (7): 04019024. https://doi.org/10.1061/(ASCE)WR.1943-5452.0001079.
Steffelbauer, D. B., J. Deuerlein, D. Gilbert, and E. Abraham. 2022. "A dual model for leak detection and localization." *J. Water Resour. Plann. Manage.* 148 (3): https://doi.org/10.1061/(ASCE)WR.1943-5452.0001515.
Stephens, M., J. Gong, and A. Marchi. 2018. "Field testing of Adelaide CBD Smart Network Acoustic Technologies." In Vol. 1 of *Proc., 1st Int. WDSA/CCWI Joint Conf.* Reston, VA: ASCE.
Taormina, R., et al. 2018. "Battle of the attack detection algorithms: Disclosing cyber attacks on water distribution networks." *J. Water Resour. Plann. Manage.* 144 (8): 04018048. https://doi.org/10.1061/(ASCE)WR.1943-5452.0000969.
Taormina, R., and S. Galelli. 2018. "Deep-learning approach to the detection and localization of cyber-physical attacks on water distribution systems." *J. Water Resour. Plann. Manage.* 144 (10): 04018065. https://doi.org/10.1061/(ASCE)WR.1943-5452.0000983.
van Thienen, P. 2021. "The hunt for leaks is on!" Accessed January 27, 2021. https://www.kwrwater.nl/actueel/the-hunt-for-leaks-is-on/.
Vftkovsky, J. P., A. R. Simpson, and M. F. Lambert. 2000. "Leak detection and calibration using transients and genetic algorithms." *J. Water Resour. Plann. Manage.* 126 (4): 262–265. https://doi.org/10.1061/(ASCE)0733-9496(2000)126:4(262).
Vrachimis, S., and D. Eliades. 2020. "The battle of the leakage detection and isolation methods 2020: Overview and results." Accessed March 15, 2021. https://doi.org/10.5281/zenodo.4139603.
Vrachimis, S. G., D. G. Eliades, R. Taormina, A. Ostfeld, Z. Kapelan, S. Liu, M. Kyriakou, P. Pavlou, M. Qiu, and M. M. Polycarpou. 2020a. "BattLeDIM: Battle of the leakage detection and isolation methods." Accessed March 13, 2021. https://doi.org/10.5281/zenodo.3902046.
Vrachimis, S. G., D. G. Eliades, R. Taormina, A. Ostfeld, Z. Kapelan, S. Liu, M. S. Kyriakou, P. Pavlou, M. Qiu, and M. Polycarpou. 2020b. "Dataset of BattLeDIM: Battle of the Leakage Detection and Isolation Methods." Accessed May 31, 2020. https://doi.org/10.5281/zenodo.4017659.
Vrachimis, S. G., M. S. Kyriakou, D. G. Eliades, and M. M. Polycarpou. 2018. "LeakDB: A benchmark dataset for leakage diagnosis in water distribution networks." In Vol. 1 of *Proc., 1st Int. WDSA/CCWI Joint Conf.* Reston, VA: ASCE.
Walski, T. 2017. "Procedure for hydraulic model calibration." *J. Am. Water Works Assn.* 109 (6): 55–61. https://doi.org/10.5942/jawwa.2017.109.0075.
Walski, T. M., D. V. Chase, D. A. Savic, W. Grayman, S. Beckwith, and E. Koelle. 2003. *Advanced water distribution modeling and management*. 1st ed. Waterbury, CT: Haestead Press.
Wang, X., G. Guo, S. Liu, Y. Wu, X. Xu, and K. Smith. 2020. "Burst detection in district metering areas using deep learning method." *J. Water Resour. Plann. Manage.* 146 (6): 04020031. https://doi.org/10.1061/(ASCE)WR.1943-5452.0001223.
Wyatt, A., J. Richkus, and J. Sy. 2016. "Using performance-based contracts to reduce nonrevenue water." In *(PPIAF Report) International bank for reconstruction and development*. Washington, DC: World Bank.
Zeng, W., A. C. Zecchin, B. S. Cazzolato, A. R. Simpson, J. Gong, and M. F. Lambert. 2021. "Extremely sensitive anomaly detection in pipe networks using a higher-order paired-impulse response function with a correlator." *J. Water Resour. Plann. Manage.* 147 (10): 04021068. https://doi.org/10.1061/(ASCE)WR.1943-5452.0001446.

Downloaded from ascelibrary.org by Andrea Cominola on 03/30/22. Copyright ASCE. For personal use only; all rights reserved.